Title: Cortical ripples provide the conditions for consolidation during NREM sleep in humans

Authors: Charles W. Dickey[1,2,*], Ilya A. Verzhbinsky[2], Xi Jiang[1], Burke Q. Rosen[1], Sophie Kajfez[3], Emad N. Eskandar[4], Jorge Gonzalez-Martinez[5], Sydney S. Cash[6], Eric Halgren[3,7,*]

Affiliations:
[1]Neurosciences Graduate Program, University of California San Diego, La Jolla, CA 92093
[2]Medical Scientist Training Program, University of California San Diego, La Jolla, CA 92093
[3]Department of Radiology, University of California San Diego, La Jolla, CA 92093
[4]Department of Neurological Surgery, Montefiore Medical Center, Albert Einstein College of Medicine, Bronx, NY 10461
[5]Epilepsy Center, Cleveland Clinic, Cleveland, OH 44106
[6]Department of Neurology, Massachusetts General Hospital, Harvard Medical School, Boston, MA 02114
[7]Department of Neurosciences, University of California San Diego, La Jolla, CA 92093

*Corresponding authors: Eric Halgren (ehalgren@health.ucsd.edu), Charles W. Dickey (cdickey@health.ucsd.edu)

Acknowledgements: We thank Adam Niese, Christine Smith, Christopher Gonzalez, Daniel Cleary, Eran Mukamel, Erik Kaestner, Jacob Garrett, Maxim Bazhenov, Terrence Sejnowski, and Zarek Siegel for their support. This work was supported by NIMH (1RF1MH117155-01, T32 MH020002) and ONR-MURI (N00014-16-1-2829).

Author contributions: C.D. and E.H. designed the study. E.E., J.G., and S.C. collected the data. C.D., I.V., and X.J. analyzed the data. B.R. and S.K. provided support for the analyses. C.D. and E.H. wrote the manuscript. E.H. supervised the work.

Competing interests: The authors declare no competing interests.

Abstract

Hippocampal ripples index the reconstruction of spatiotemporal neuronal firing patterns essential for the consolidation of memories in the cortex during non-rapid eye movement (NREM) sleep. However, it is not known whether ripples are generated in the human cortex during sleep. Here, using human intracranial recordings, we show that ~70ms long ~80Hz ripples are ubiquitous in all regions of the cortex during NREM sleep as well as waking. During waking, cortical ripples occur on local high frequency activity peaks. During sleep, cortical ripples occur during spindles on the down-to-upstate transition, with unit-firing patterns consistent with generation by pyramidal-interneuron feedback. Cortical ripples mark the recurrence of spatiotemporal activity patterns from preceding waking, and they group co-firing within the window of spike-timing-dependent plasticity. Thus, cortical ripples guided by sequential sleep waves may facilitate memory consolidation during NREM sleep in humans.

Introduction

Ripples have been extensively studied in rodent hippocampus during non-rapid eye movement (NREM) sleep, when they mark the replay of events from the prior waking period, and are critical for memory consolidation in the cortex[1-4]. They are associated with cortical replay[5-7], and with cortical sleep waves (spindles, downstates, upstates)[8], a relationship crucial for consolidation[9]. Rat hippocampal ripples comprise a ~140Hz oscillation at the peak of a ~70ms duration sharpwave, followed by a slower local potential[2]. Human hippocampal sharpwave-ripples also occur during NREM sleep with similar temporal relationships to spindles and down-to-upstates and hippocampal topography, but with a median frequency of 80-90Hz[10-13].

Recently, ripples were found in rat association cortex but not primary sensory or motor cortices during sleep, with increased coupling to hippocampal ripples in sleep following learning[14]. An earlier study reported ripples in waking and sleeping cat cortex, especially during NREM sleep[15]. In humans, cortical ripples during waking were more frequently found in lateral temporal than rolandic cortex, and coupled to parahippocampal gyrus ripples more often prior to correct paired-associates recall[16]. Lateral temporal units fired in-phase with the local ripples in patterns previously observed during learning[17]. Waking hippocampal ripples were also associated with cortical activity patterns selective for faces and buildings during free recall[18].

Thus, there is an emerging appreciation that, in humans and rodents, hippocampal and cortical ripples play an important role in memory during both sleep and waking. However, many fundamental questions remain unresolved, including whether cortical ripples are generated during sleep in humans. The basic characteristics of ripples have not been compared between cortex and hippocampus, or between sleep and waking, so it is unclear how ripples may differ between their putative roles of supporting consolidation vs. recall, or indeed if they represent the same phenomenon. Knowledge of the distribution of ripples across different cortical areas during waking is limited and during sleep is absent. The relations between cortical ripples and sleep spindles, downstates, and upstates have not been determined. Such relations could support a role of cortical ripples in consolidation, as would increased unit pair co-firing within the window of spike-timing-dependent plasticity (STDP), as well as association with spatiotemporal activity patterns identified during waking that ‘replay’ during subsequent sleep. Furthermore, the relationships of human cortical pyramidal and inhibitory cell-firing to ripples and to each other, important for understanding ripple generation, have not been determined.

Here, using intracranial stereoelectroencephalography (SEEG) recordings, we provide the first demonstration that cortical ripples are generated during NREM sleep in humans, and we make the first comprehensive characterization of ripples throughout the cortex during waking and NREM sleep. We show that cortical ripples in NREM sleep couple to spindles and down-to-upstates with timing that could support consolidation, and to spatiotemporal patterns that recur from preceding waking, suggesting a possible role for ripples in memory replay. Using single-unit recordings from cortical microarrays, we identify the probable generating circuits of cortical ripples and show that units co-fire during ripples at short delays that are optimal for STDP. Thus, cortical ripples have the necessary physiological properties to facilitate replay-guided plasticity during non-rapid eye movement sleep in humans.

Results

Ripples are generated across states and structures

Ripples were detected using intracranial cortical and hippocampal stereoelectro-encephalography (SEEG) recordings in 17 patients undergoing monitoring for seizure focus localization (STable 1). Bipolar derivations ensured measurement of local field potentials (LFP). Ripples were detected exclusively from non-lesional, non-epileptogenic regions and were required to have at least 3 cycles of increased 70-100Hz amplitude without contamination by epileptiform activity or artifacts (SFig.1). Ripples were found during both waking and NREM sleep in all cortical areas sampled (Fig.1A-B,E-H, Table 1, SFig.2), and hippocampus (Fig.1C-D).

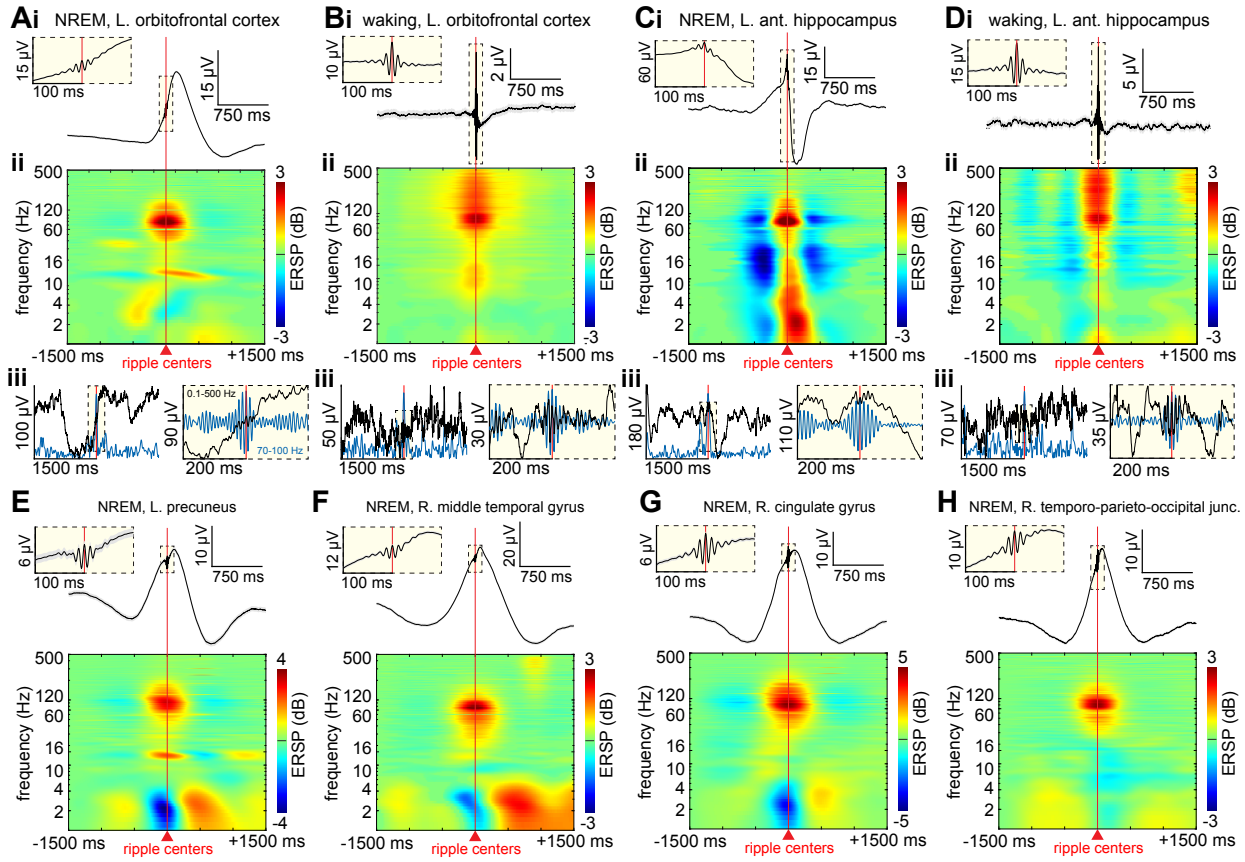

Fig. 1. Cortical and hippocampal ripples are generated during NREM sleep and waking. (**A**) Orbitofrontal average broadband LFP (**i**) and time-frequency (**ii**) across ripples, and example broadband ripple (**iii**) broadband sweeps (black, left–3000ms, right–400ms), and 70-100Hz bandpass (blue, left-analytic amplitude, right-sweep), from one channel during NREM sleep. Note the increased power in the 10-16Hz spindle band coinciding with the ripples. (**B**) Same as (A) except during waking. (**C**) Same as (A) except hippocampal ripples. (**D**) Same as (C) except during waking. (**E-H**) Same as (A) except for other cortical regions. Note the highly consistent occurrence of cortical ripples on the down-to-upstate transition during NREM sleep. All plots show ripples detected on trans-gray matter bipolar SEEG channels. LFP=local field potential, NREM=non-rapid eye movement, SEEG=stereoelectroencephalography.

Cortical Region	No. Chan	No. Ripples		Density (min^{-1})		Amplitude (μV)		Frequency (Hz)		Duration (ms)	
		Sleep	Waking	Sleep	Waking	Sleep	Waking	Sleep	Waking	Sleep	Waking
Orbitofrontal	14	129680	211957	9.01±2.74	4.83±3.26	1.31±0.26	2.26±1.21	80.3±0.4	80.8±0.7	64.1±4.5	57.8±3.0
Prefrontal	37	287124	609692	9.28±2.66	6.62±3.11	1.62±0.57	2.10±0.82	80.7±0.5	81.0±0.5	62.4±3.9	56.7±2.7
Rolandic	25	174262	315588	8.84±2.57	6.7±3.23	1.82±0.91	2.57±1.43	81.2±0.9	81.3±0.6	63.9±5.5	57.8±3.3
Parietal	79	491431	855766	8.18±2.68	5.17±3.45	1.76±0.64	2.44±1.09	81.3±0.7	81.3±0.5	65.5±6.6	58.2±3.7
Occipital	14	94144	103609	8.71±2.91	4.55±3.8	1.95±0.74	2.99±1.21	81.5±0.4	81.3±0.4	68.3±5.7	57.4±3.0
Superior Temporal / Insula	20	182981	324005	8.99±2.08	7.90±4.15	1.50±0.61	2.39±1.29	80.8±0.7	81.2±0.6	64.0±7.2	57.1±3.2
Lateral Temporal	47	295324	534754	6.89±2.61	4.95±3.35	1.23±0.71	1.89±1.34	80.7±0.9	81.2±0.7	63.6±8.4	58.0±3.4
Ventral Temporal	34	224478	415057	8.58±2.64	6.54±2.82	1.85±0.78	2.60±1.67	81±0.9	81.2±0.7	66.9±5.6	61.1±6.5
Cingulate	3	27078	42804	9.31±1.84	7.00±2.17	1.19±0.79	1.49±0.92	82.5±2.8	82.5±2.0	68.3±8.6	74.3±30.2
Hippocampus	28	147138	409734	6.95±4.80	7.40±5.50	5.79±2.99	5.25±3.01	78.9±4.4	80.5±4.4	85.0±34.9	69.6±28.6

Table 1. Cortical and hippocampal ripple characteristics by region in NREM sleep and waking. Cortical parcellation scheme is specified in STable 6. Values are counts or means and standard deviations across channels from SEEG patients S1-17.

Across states and structures, ripple frequency was remarkably consistent (~80Hz), durations were similar (~70ms), and spontaneous cortical ripple occurrence rate was higher during NREM sleep than waking (Figs.2-3). Recording epochs and channels with possible contamination by epileptiform activity were rigorously rejected, and these basic ripple characteristics were very similar when only cortical or hippocampal channels free of interictal spikes were analyzed (SFig.1B-C). Previous work in sleeping rats[14] and waking humans[16] found cortical ripples to be absent or infrequent in early sensory and motor as compared to association areas. In contrast, we found that ripple density, amplitude, and accompanying >200Hz amplitude (a proxy for unit-firing[19]), were all lower in association areas, as indicated by a positive correlation with the myelination index[20] (Fig.3G-H, SFig.3).

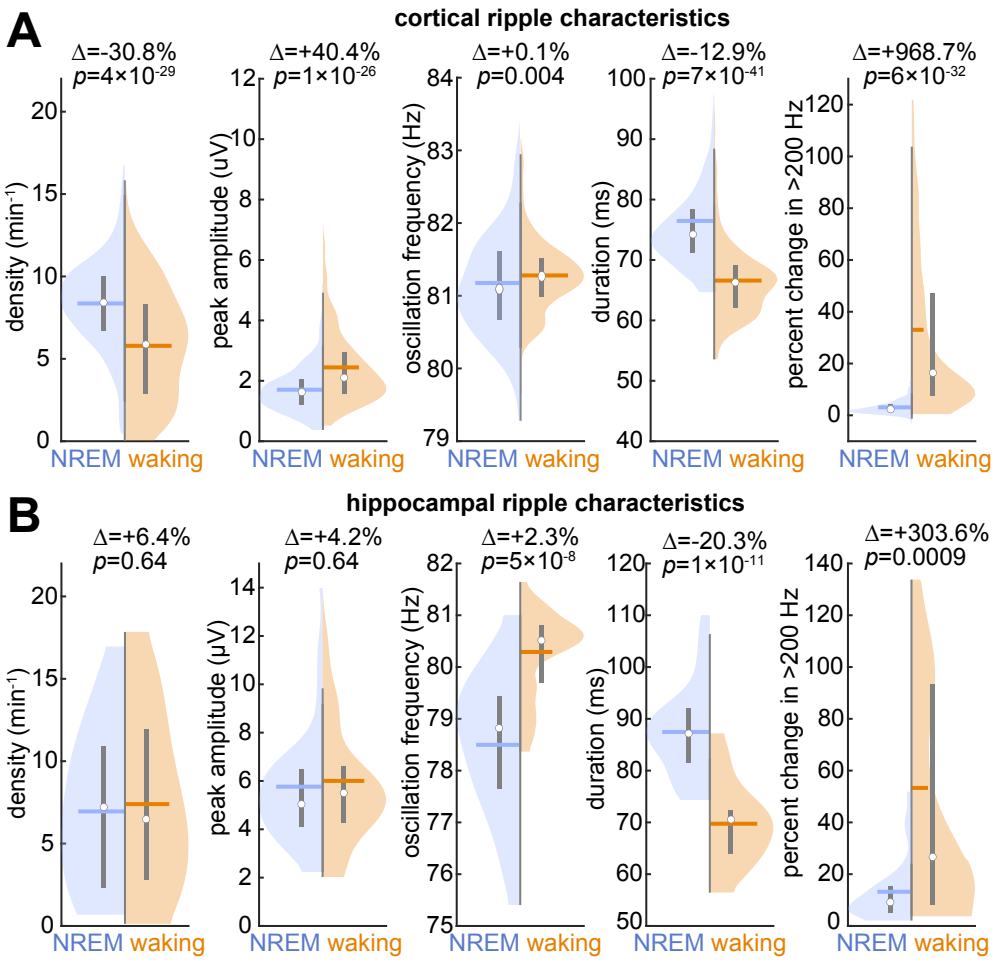

Fig. 2. Cortical and hippocampal ripple characteristics in NREM sleep and waking. (**A**) NREM sleep vs. waking cortical ripple density, peak 70-100Hz amplitude, frequency, duration, and percent change in mean >200Hz amplitude during ripples compared to a -2 to -1s baseline (*N*=273 channels; SEEG patients S1-17). (**B**) Same as (A) except hippocampal ripples (*N*=28 channels). Circles show medians; horizontal lines, means; vertical lines, interquartile ranges. FDR-corrected *p*-values, two-sided paired *t*-test. FDR=false discovery rate.

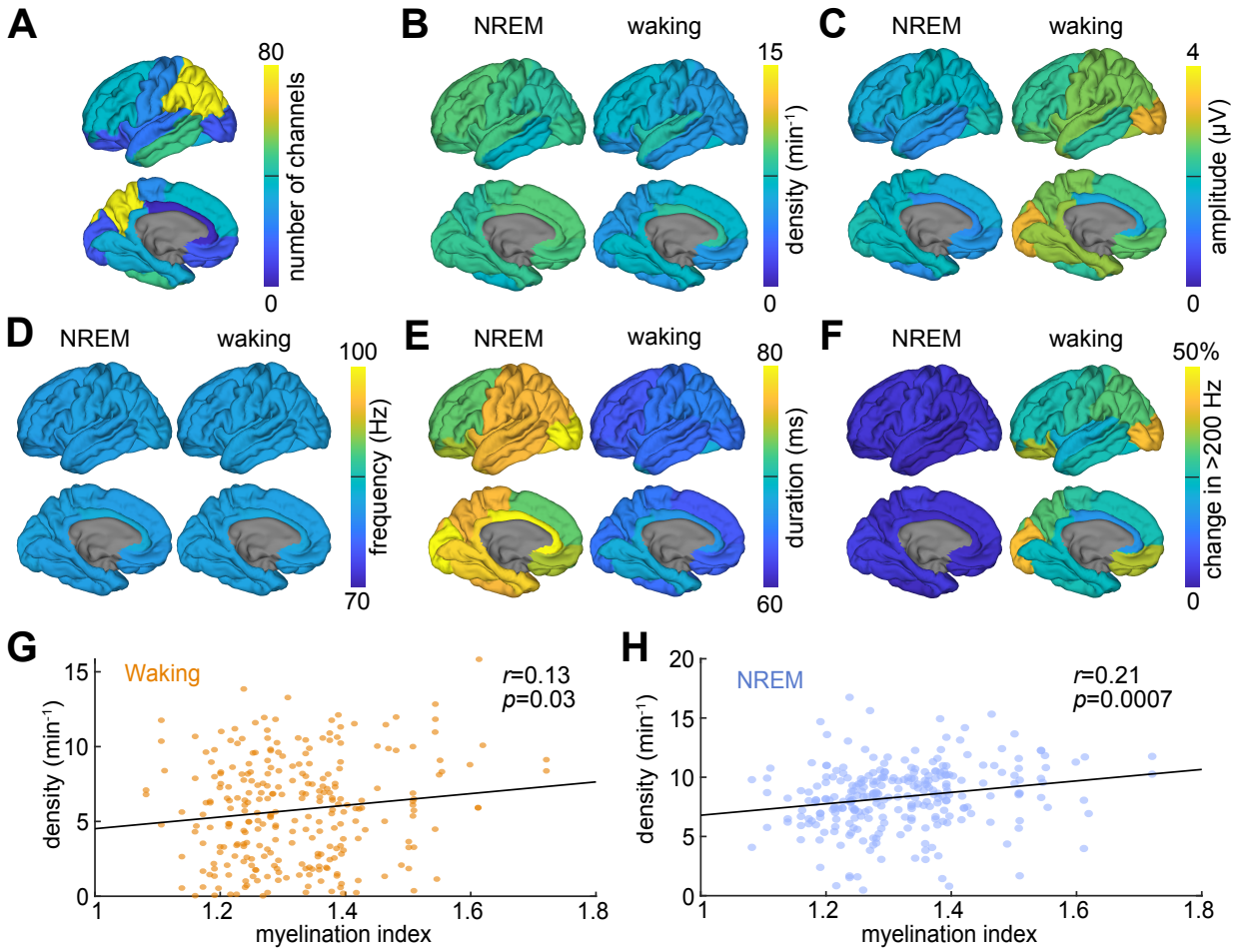

Fig. 3 Distributions of ripple characteristics across the cortex in NREM sleep and waking. (**A-F**) Cortical maps of channel coverage (**A**) as well as mean ripple densities (**B**), amplitudes (**C**), frequencies (**D**), durations (**E**), and changes in mean >200Hz analytic amplitude during ripples compared to baseline (-2 to -1s) (**F**) during NREM sleep and waking (*N*=273 channels; SEEG patients S1-17). Left and right hemisphere channels were combined and mapped onto a left hemisphere template brain. Parcellation scheme is specified in STable 6. Values for each cortical region are reported in Table 1. (**G-H**) Cortical ripple density was positively correlated with cortical parcel myelination index (i.e., lower densities in association compared to primary areas[20]) during waking (**G**) and NREM sleep (**H**). Amplitude and oscillation frequency during waking and NREM sleep, and change in >200Hz amplitude during NREM sleep also had significant positive linear correlations, but duration in either state and change in >200Hz amplitude during waking were non-signiifcant (SFig.3).

Cortical ripples lock to sleep waves crucial for memory consolidation

NREM sleep is characterized by large downstates, often followed by upstates with spindles[21,22]. Hippocampal ripples tend to occur on the cortical down-to-upstate transition with spindles in rodents[7,8] and humans[10,11]. These precise oscillation couplings are important for memory consolidation[9]. Previous studies have shown that cortical ripples occur on upstate and spindle peaks in cats[15] and rats[14], but these relationships have not been evaluated in humans. We detected downstates, upstates, and spindles (STable 2) and found that cortical ripples were precisely coupled to the sequence of sleep waves described above. Specifically, cortical ripples

were generated on the down-to-upstate transition (Fig.1A,E-H, Fig.4A-B,D, SFig.2A), often on spindles (Fig.1A,E, Fig.4A,C, STable 3), with a preference for spindles preceding upstates (Fig.4E). These results suggest that cortical ripples may help to facilitate consolidation, guided by a sequential activation of sleep waves.

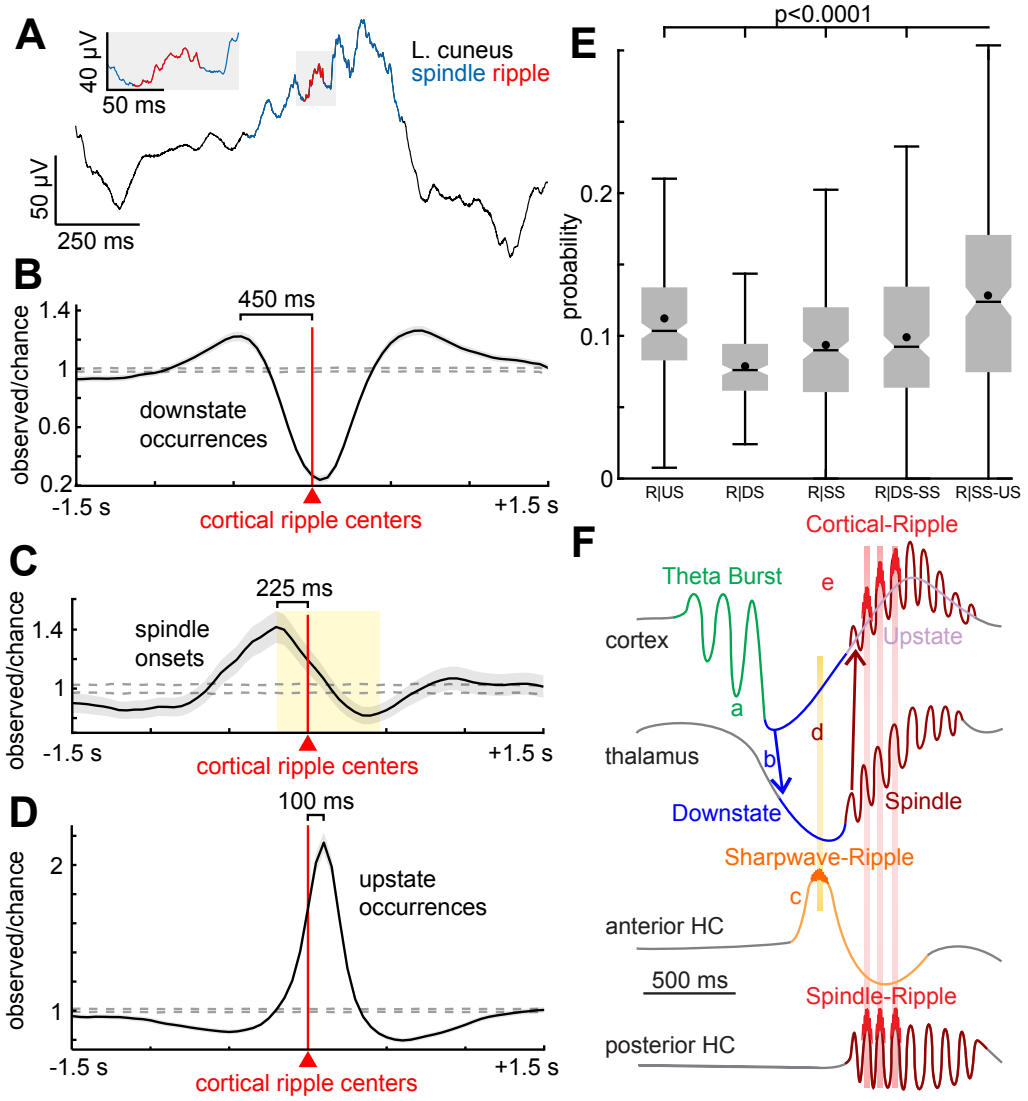

Fig. 4. Cortical ripples occur during sleep spindles on the down-to-upstate transition. (**A**) Example cortical ripple occuring during a spindle on a down-to-upstate transition. (**B**) Smoothed histogram shows average downstate peak times plotted relative to local cortical ripple centers at *t*=0 across significant channels (*N*=258/273, patients S1-17). Dashed lines show 99% confidence interval of the null distribution (200 shuffles/channel). (**C-D**) Same as (B) except spindle onsets (*N*=80/273) (**C**) with shaded area indicating average spindle duration, and downstate peaks (*N*=260/273) (**D**). (**E**) Probabilities of ripple centers (R) preceding upstates (US), following downstates (DS), or occurring during spindles (SS), spindles following downstates (DS-SS), or spindles preceding upstates (SS-US; *N*=212 channels from patients S1-17; minimum 20 events of each type required per channel). The time window used following downstates or preceding upstates was 634ms, which was the average spindle duration. The probability of a ripple occurring was greatest during spindles preceding upstates (post-FDR

$p<0.0001$, paired two-sided *t*-test). (**F**) Timing of ripples, spindles, and down-to-upstates across structures. A cortical theta burst leads to a downstate[21] (*a*) which triggers a thalamic-downstate (*b*) and rebound hippocampal sharpwave-ripple[11] (*c*) arriving at the cortex rebooting from its downstate; meanwhile, the thalamic-downstate enables h and T currents to generate a spindle projected to the cortex[22] (*d*) with phase-locked posterior hippocampal spindle-ripples[12]. Overall, cortical ripples during NREM sleep occur on the down-to-upstate slope, often during spindles (*e)*. HC=hippocampus.

Pyramidal cell firing precedes interneuron firing at cortical ripple peaks

Using microelectrode array recordings from granular/supragranular layers of lateral temporal cortex during NREM sleep, we detected ripples (Fig.5A) as well as action-potentials, which were sorted into those arising from putative single pyramidal cells or interneurons (SFig.4, STable 4). We found that interneurons showed a strong tendency to fire at the peak of the ripple, whereas pyramidal cells fired shortly before (Fig.5B). We have previously shown that, in humans, upstates[23] and spindles[24] are associated with increased unit-firing rates. Since cortical ripples are precisely coupled to these events (Fig.4), their occurrence on upstates and spindles implies an underlying phasic depolarization, which can generate ~80Hz oscillations in computational and experimental models via pyramidal-interneuron feedback inhibition[2,25]. Depolarization causes basket cells to fire synchronously, inhibiting other basket cells and pyramids via $GABA_A$. Pyramids fire upon recovery, exciting basket cells as they recover, leading to another cycle. As this model would predict, we found that pyramids and interneurons were strongly phase-locked to cortical ripples (Fig.5B-C), with pyramidal significantly leading interneuron spiking (Fig.5D). Furthermore, interneurons fired at ripple peak, when pyramidal somatic inhibition would be maximal, as found in cats[15]. Similarly, ripple amplitude was higher in waking than NREM sleep (Figs.2B, 3C), consistent with relative depolarization of pyramidal membrane potential during waking. Phasic depolarization during waking ripples was also suggested by increased >200Hz amplitude (Figs.2, 3F). Thus, human cortical ripples are associated with strong tonic and phase-locked increases in pyramidal and interneuron firing, and are likely generated by a sudden depolarization triggering pyramidal-interneuron feedback oscillations (Fig.5E).

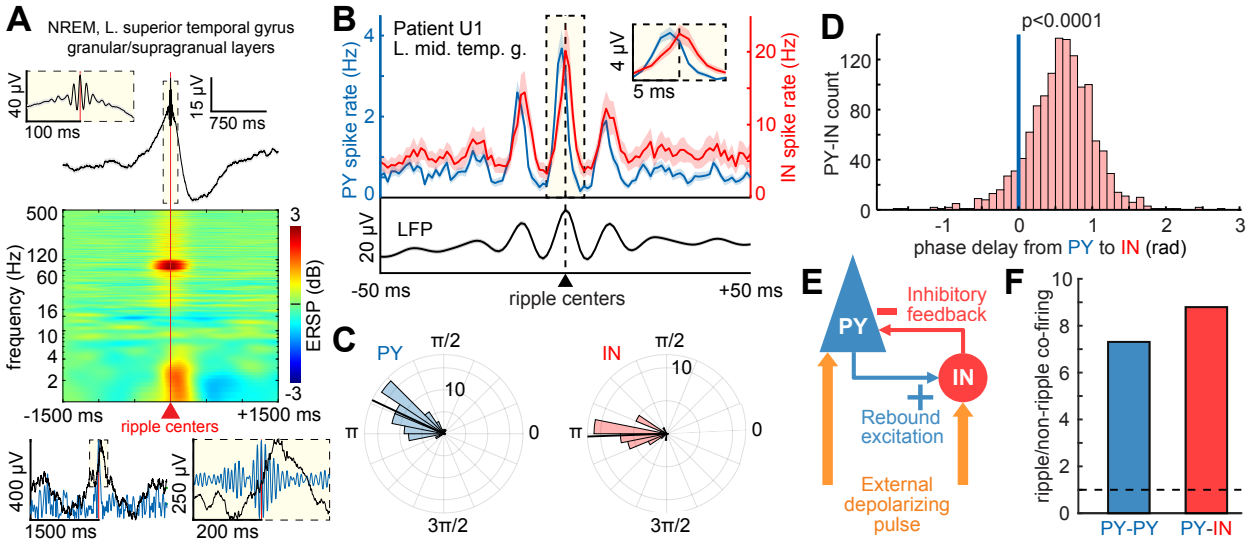

Fig. 5. Pyramidal cell firing leads interneuronal at cortical ripple peaks. (**A**) Superior temporal gyrus granular/supragranular layer ripples detected during NREM sleep in a Utah Array recording. Top shows average broadband LFP, middle shows average time-frequency, and bottom shows single trial example trace in broadband LFP (black) and 70-100Hz bandpass (blue, left–analytic amplitude, right–sweep). (**B**) Mean broadband LFP locked to cortical ripple centers (black) and associated local PY (N=69) and IN (N=23) spike rates during NREM sleep. (**C**) Circular mean 70-100Hz phase of spikes of each PY (N=73, mean=2.70rad, $p=2\times10^{-7}$, Hodges-Ajne test) and IN (N=36, mean=3.18rad, p≈0) during local cortical ripples (minimum 30 spikes per unit). PY spiking preceded IN spiking by 0.48rad ($p=2\times10^{-7}$, Watson-Williams test). (**D**) Circular mean ripple phase-lags of spikes from each PY (N=73) to each IN (N=36) (N=1280 unit pairs, mean=0.58±0.46rad, $p=1\times10^{-268}$, one-sample one-sided t-test). (**E**) Pyramidal Interneuron Network Gamma ripple generation mechanism consistent with single-unit recordings, animal studies[26], and modelling[27]. Abrupt depolarization causes synchronous PY and IN firing, which then spike rhythmically separated by fixed intervals due to recurrent inhibition. (**F**) Pairs of pyramidal cells (PY-PY) co-fire ~7 times more often within 5ms of each other during ripples compared to randomly selected epochs in between ripples matched in number and duration to the ripples. Similarly, pyramidal-interneuron (PY-IN) pairs co-fire ~9 times more during ripples. IN=putative interneuron, PY=putative pyramidal.

Cortical ripples group co-firing with timing optimal for spike-timing-dependent plasticity

The increased phase-locked unit firing and occurrence of ripples on spindles on the down-to-upstate transition suggest that ripples may facilitate cortical plasticity[24]. This could occur through short latency co-firing between units that leads to STDP. Indeed, we found a large increase during ripples of short latency (<5ms) co-firing between pyramidal-pyramidal unit pairs and pyramidal-interneuron unit pairs (Fig.5F). Specifically, there was an increase in co-firing during ripples vs. non-ripples (PY-PY: 7.31 fold increase, $p=6\times10^{-193}$, N=7846, t=30.5; PY-IN: 8.79 fold increase, $p=1\times10^{-177}$, N=2113, t=29.0; paired two-sided t-test). Non-ripple comparison periods were randomly selected epochs between ripples matched in number and duration. There was also a significant increase in short-latency co-firing in actual ripples, as compared to co-firing when the spike times within the ripples were randomly shuffled (PY-PY: 1.27 fold increase, $p=3\times10^{-12}$, N=7846, t=7.0; PY-IN: 1.18 fold increase, $p=2\times10^{-15}$, N=2113, t=7.9; paired two-sided t-test). This latter finding indicates that the increase in co-firing is not simply due to an increase in the overall firing rates of units during ripples, or even their rhythmicity, but rather a specific

organization of co-firing by the phase of individual ripple cycles. Thus, ripples create a necessary and sufficient condition for STDP, and therefore may underlie the crucial contribution of these nested waves to consolidation[24].

Cortical ripples mark 'replay' of spatiotemporal activity patterns

Hippocampal ripples in NREM sleep mark the assembly of spatiotemporal firing patterns reproducing the sequential attributes of events from the preceding waking, supporting cortical replay and consolidation[2,28]. However, cortical ripples have not been associated with replay during NREM sleep. Our group previously identified waking spatiotemporal patterns of high gamma (70-190Hz) activity across widespread cortical areas that recurred more often in the following compared to preceding sleep nights (Fig.6A). These events also coupled to upstates, spindles and hippocampal ripples[29]. In new analyses of these data (STable 5), we found that the high gamma events that comprised these sequences of putative replay were strongly linked to cortical ripples (Fig.6B-E), supporting the possibility that cortical ripples contribute to replay underlying the consolidation of memories in the cortex.

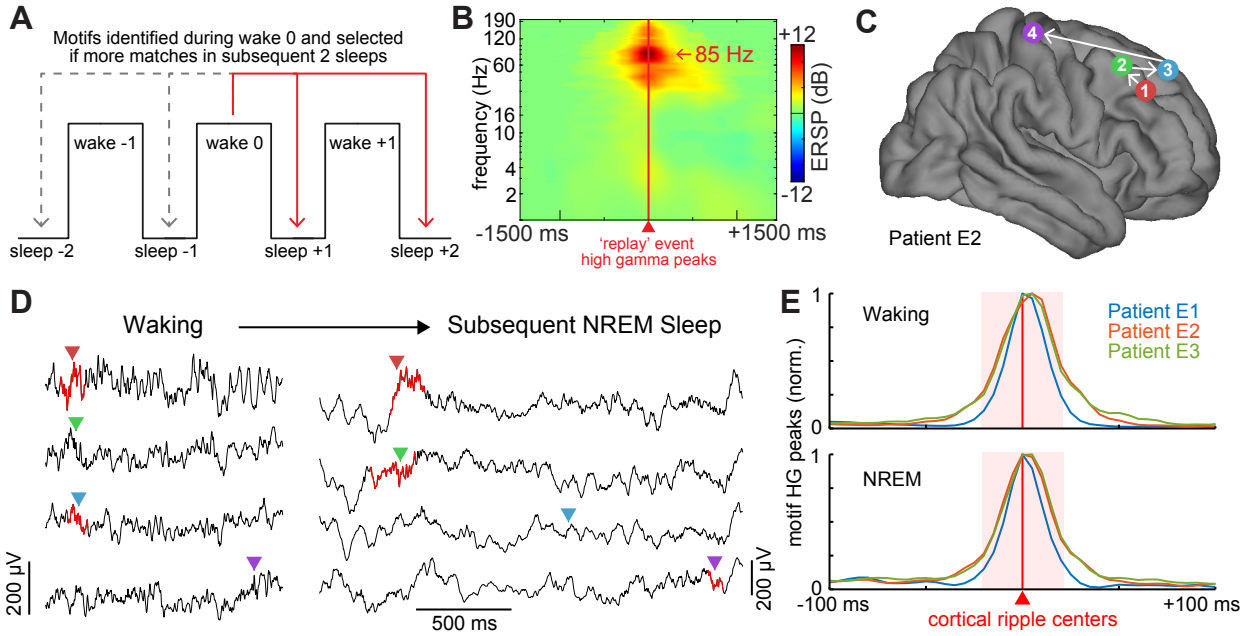

Fig. 6. Cortical ripples during NREM sleep are associated with spatiotemporal activity patterns that recur from previous waking. (**A**) Schematic for comparing the number of matching spatiotemporal patterns ('Motifs') of high gamma (70-190Hz) peaks from waking to preceding versus subsequent 2 sleeps[29]. All 3 patients had significantly more waking Motif matches to the subsequent compared to the preceding 2 sleeps (p<0.00001, two-sided binomial test, expected value=0.5). Events that were "exact matches" (i.e., common channels had same temporal order), which occurred more during the subsequent compared to the preceding 2 sleeps, were selected to test if they were related ripples. (**B**) Average time-frequency plot centered on Motif high gamma peaks shows focal activation in the ripple band. (**C-D**) Spatiotemporal high gamma peak sequence from an example Motif superimposed on a template brain (**C**) and as broadband LFP traces with ripples indicated in red (**D**). (**E**) Average Motif high gamma peak times plotted relative to local cortical ripple centers.

Discussion

The current study provides the first comprehensive characterization of cortical ripples during waking and NREM sleep and provides the first evidence for their role in memory consolidation in humans. Using intracranial recordings, we report that human cortical ripples are widespread during NREM sleep in addition to waking. Basic ripple characteristics (occurrence rate, amplitude, oscillation frequency, duration, distribution across cortical areas) are very similar in cortex vs. hippocampus, and NREM sleep vs. waking. These characteristics are similar to those of rodents with two exceptions. First, the center frequency of human ripples is ~80Hz[11], whereas in rodents it is ~130Hz[2]. Conceivably, the larger human brain may require more time for cortico-cortical and hippocampo-cortical integration than the rodent brain. The second apparent difference between humans and rodents is in cortical distribution. A previous rodent study found that cortical ripples were restricted to association cortex[14], and consistent observations were reported in humans[16]. In contrast, we recorded cortical ripples in all areas sampled, with approximately equal occurrence rates that were lower in association areas as indicated by the positive correlation between occurrence rate and myelination index.

In contrast to the similarity of basic properties, we found that ripples in waking vs. NREM sleep occur within much different immediate physiological contexts. In NREM sleep, cortical ripples are strongly associated with local upstates, downstates, and sleep spindles. Characteristically, ripples occur on the upslope ~100ms before the peak of the upstate. Previous studies found that sleep spindles[24] and upstates[23] are associated with strong increases in local unit-firing, and we found that also to be the case for cortical ripples during NREM sleep. Hippocampal ripples during NREM sleep in previous studies were also found to often occur during local sharpwaves or spindles[10-13].

Of course, sleep spindles and down-to-upstates are characteristic of NREM sleep and would not be expected to occur with waking ripples. In addition, during waking, we found no other lower-frequency wave to be consistently associated with ripples. However, both cortical and hippocampal ripples occurred during greatly increased local >200Hz amplitude activity, a surrogate for unit-firing[19]. Thus, the local contexts of both cortical and hippocampal ripples, in both NREM and waking, are sudden increases in local excitability lasting ~70ms. NREM and waking are different in that the depolarizing pulse is organized by endogenous sleep rhythms in NREM, but appears to be related to exogenous input, such as a retrieval cue, during waking.

Computational neural models and experimental studies have found that depolarizing pulses can induce oscillations from ~20-160Hz[2,27]. Depolarization causes synchronous pyramidal cell firing, which is inhibited for a fixed time by recurrent inhibition from local basket cells. The pyramidal cells then fire again, resulting in Pyramidal Interneuron Network Gamma (PING). As predicted by this model, we found strong ripple phase-modulation of putative pyramidal and interneuronal firing, with pyramids regularly preceding interneurons. Our findings are also consistent with PING supplemented by synchronized basket cell firing and mutual inhibition (ING; Interneuron Network Gamma)[30]. Definitive mechanistic demonstration would require experiments not currently possible *in vivo* in humans[26].

A critical aspect of hippocampal-dependent declarative memory is the linkage of novel constellations of elements encoded in widespread cortical locations. Thus, for replay to facilitate consolidation, it must re-activate spatiotemporal patterns distributed across the cortex. Previously, we showed that widespread spatiotemporal high gamma patterns from waking recur more during subsequent than preceding NREM sleep[29]. Here, we found that the activity peaks

that form these patterns are tightly coupled with cortical ripples, consistent with ripples having a role in recurrence and potentially replay.

Consolidation requires plasticity as well as replay to increase the strength of the connections embodying the memory. The prime candidate is STDP, which occurs when pre- and post-synaptic cells fire in close temporal proximity[31]. We show here that local neurons are much more likely to fire at delays optimal for STDP during ripples than control periods, and that co-firing is organized beyond what would be expected by a general increase in neuron firing. A similar increase is also observed during spindles and upstates in humans[24]. Since we also show that NREM cortical ripples are temporally coordinated with spindles and upstates, this supports a synergistic facilitation of plasticity.

In summary, the current study provides the first report of cortical ripples during sleep in humans. Cortical ripples during NREM sleep were found to have basic characteristics (duration, oscillation frequency, occurrence rate, and widespread cortical distribution) that are very similar to those of cortical ripples during waking as well as hippocampal ripples. Unit-firing during human cortical NREM ripples supported the mechanism proposed for rodent hippocampal ripples, based on pyramidal-interneuron feedback. Cortical ripples during NREM characteristically occurred after downstates, during spindles, shortly before the peak of the upstate, an association and timing important for consolidation of memories during NREM sleep. Furthermore, NREM cortical ripples occurred at the peaks of spatiotemporal activation patterns that recurred from waking, and modulated paired cell-firing so that they fulfilled a basic requirement for STDP. Overall, these results are consistent with human cortical ripples playing a key role in consolidation during NREM sleep.

Methods

Patient selection

Data from a total of 21 patients (13 female, 32±13 years old) with pharmaco-resistant epilepsy undergoing intracranial recording for seizure onset localization preceding surgical treatment were included in this study (STables 1, 4, 5). Patients whose stereoelectroencephalography (SEEG) recordings were analyzed were only included in the study if they had no prior brain surgery; background EEG (with the exception of epileptiform transients) in the normal range; and electrodes implanted in what was eventually found to be non-lesional, non-epileptogenic cortex, as well as non-lesional, non-epileptogenic hippocampus (such areas were suspected to be part of the focus prior to implantation, or were necessary to pass through to reach suspected epileptogenic areas). In 3 of these patients, previously collected electrocorticography (ECoG; subdural grids and strips) recordings were analyzed.

Furthermore, 3 of these patients undergoing electrocorticography and SEEG recording for the clinical purpose of seizure localization were also implanted with an intracranial microelectrode (Utah Array) into tissue that was suspected based on pre-surgical evaluation to be included within the region of the therapeutic resection. The implantation of the array did not affect clinical monitoring. In every case, the tissue into which the array was implanted was later resected in order to gain access to the surgical focus beneath. In all of these patients the electrode was determined not to be implanted in an epileptogenic zone, and no seizures originated from the region of the array in any of the patients.

Patients were excluded from the study if they had prior brain surgery or did not have non-lesioned hippocampal and cortical channels that were not involved in the early stage of the

seizure discharge and did not have frequent interictal activity or abnormal local field potentials. Based on these criteria, 21 were included in this study out of a total of 84. All patients gave fully informed written consent for their data to be used for research as monitored by the local Institutional Review Boards at Cleveland Clinic and Partners HealthCare (including Massachusetts General Hospital).

Intracranial recordings

Patients were implanted with intracranial electrodes for ~7 days with continuous recordings for seizure onset localization. SEEG and ECoG electrode implantation and targeting were made for purely clinical purposes. SEEG recordings (*N*=17 patients) were collected with a Nihon Kohden JE-120 amplifier at 1000Hz sampling (patients S1-17). Standard clinical electrodes were 0.8mm diameter, with 10-16 2mm long contacts at 3.5-5mm pitch (~150 contacts/patient). ECoG recordings were collected at 500Hz (patient E1) or 512Hz (patients E2-3) using 128-channel clinical cable telemetry systems (STable 5).

Microelectrode recordings from 3 patients implanted with a Utah Array were also analyzed (STable 4). The Utah Array is a 10x10 microelectrode array with corners omitted and 400μm contact pitch[32-34]. Each silicon probe is 1 or 1.5mm long with a base of 35-75μm that tapers to 3-5μm. The probes are insulated except for the platinum-coated tip. Data were acquired at 30kHz (Blackrock Microsystems) with a 0.3-7.5kHz bandpass. Data were referenced with respect to a distant reference wire.

Electrophysiology pre-processing

Offline data preprocessing was performed in MATLAB 2019b and LFPs were inspected visually using the FieldTrip toolbox[35]. SEEG data were downsampled to 1000Hz with anti-aliasing and 60Hz notch filtered (zero-phase) with 60Hz harmonics up to 480 Hz. Transcortical contact pairs were identified using both anatomical location (using the pre-operative MRI aligned to the post-operative CT), and physiological properties (high amplitude, coherence and inversion of spontaneous activity between contacts), and selected such that no 2 pairs shared a contact. All SEEG analyses were done using bipolar derivations of adjacent contacts in cortical or hippocampal gray matter in order to ensure that activity was locally generated[36].

Channel selection

Channels were excluded from the study if they were in lesioned tissue, involved in the early stages of the seizure discharge, had frequent interictal activity, or abnormal local field potentials. From the total 2129 bipolar channels (1202 left hemisphere) in the 17 SEEG patients (S1-17), 28 hippocampal (16 left hemisphere) and 273 transcortical (133 left hemisphere) bipolar channels were selected for the analyses (STable 1). Polarity was corrected for individual bipolar channels such that downstates were negative and upstates were positive. This was accomplished by ensuring that during NREM sleep, negative peaks were associated with decreased and positive peaks were associated with increased mean ±100ms 70-190Hz analytic amplitude, an index of cell-firing that is strongly modulated by downstates and upstates[23].

Electrode localization

Cortical surfaces were reconstructed from the pre-operative whole-head T1-weighted structural MR volume using the standard FreeSurfer recon-all pipeline[37]. Atlas-based automated parcellation[38] was used to assign anatomical labels to regions of the cortical surface in the

Destrieux[39] atlas. In addition, automated segmentation was used to assign anatomical labels to each voxel of the MR volume, including identifying voxels containing hippocampal subfields[40]. In order to localize the SEEG contacts, the post-implant CT volume was registered to the MR volume, in standardized 1mm isotropic FreeSurfer space, using the general registration module[41] in 3D Slicer[42]. The position of each SEEG contact, in FreeSurfer coordinates, was then determined by manually annotating the centroids of electrode contact visualized in the co-registered CT volume. Each transcortical contact pair was assigned an anatomical parcel from the atlas above by ascertaining the parcel identities of the surface vertex closest to the contact-pair midpoint. Subcortical contacts were assigned an anatomical label corresponding to the plurality of voxel segmentation labels within a 2-voxel radius. Transcortical contact pair locations were registered to the fsaverage template brain for visualization by spherical morphing[43]. To plot values on a template brain, channel means were averaged for each cortical region (with the two hemispheres combined) and then morphed onto a left hemisphere ico5 fsaverage template. Cortical regions are amalgamations of the Desikan parcels[44] as specified in STable 6.

Myelination indices

A cortical area's hierarchical position is inversely proportional to its degree of myelination and this is indexed by the ratio between T1-weighted and T2-weighted MRI contrast[45]. Group average (N=1065 healthy young adults) myelination indices for each of the 360 parcels in the HCP-MMP1.0 atlas[46] were previously obtained using the Human Connectome Project dataset[20]. These indices were then assigned to SEEG bipolar channels based on the HCP parcel in which they were located.

Time-frequency analyses

Average time-frequency plots of the ripple event-related spectral power (ERSP) were generated from the broadband LFP using EEGLAB[47]. Event-related spectral power was calculated from 1Hz to the Nyquist frequency (500Hz except for 250Hz in patient E1 and 256Hz in E2-3) with 1Hz resolution with ripple centers at t=0 by computing and averaging fast Fourier transforms with Hanning window tapering. Each 1Hz bin of the time-frequency matrix was normalized with respect to the mean power at -2000 to -1500ms and masked with two-tailed bootstrapped significance (N=200) with FDR correction and α=0.05 using -2000 to -1500ms as baseline.

Sleep and waking epoch selection

Epochs included in the study did not fall within at least 1 hour of a seizure and were not contaminated with frequent interictal spikes or artifacts. NREM sleep periods were selected from continuous overnight recordings where the delta (0.5-2Hz) analytic amplitude from the cortical channels was persistently increased (STable 1). Sleep epochs were confirmed by visual inspection to have normal appearing spindles, downstates, and upstates. Spindles, downstates, and upstates were also automatically detected (see "Sleep graphoelement detection"), and quantification of these events showed they had densities, amplitudes, and frequencies characteristic of NREM sleep (STable 2). Waking periods were selected from continuous daytime recordings that had persistently low cortical delta as well as high cortical alpha (8-12 Hz), beta (20-40Hz), and high gamma (70-190Hz) analytic amplitudes. When the data included electrooculography (EOG; N=15/17 SEEG patients), waking periods also required that the 0.5-40Hz analytic amplitude of the EOG trace was increased. Waking epochs were required to be separated from periods of increased delta by at least 30 minutes.

Ripple detection

The median center frequency of hippocampal ripples in 9 studies was ~85Hz in humans[10,12,16,18,48-52], whereas in rodents, sharpwave-ripple frequency is ~120-140Hz. In humans, putative 80Hz hippocampal ripples have the same characteristic relation to sharpwaves, intra-hippocampal localization, modulation by sleep stage, and relation to cortical sleep waves as in rodents, and occur in hippocampi that have no signs of epileptic involvement. Furthermore, in rodent hippocampus the distinction between higher frequency gamma bursts and ripples is not always sharp, leading to the suggestion that for simplicity they both be referred to as 'ripples'[26], which we follow here.

Ripple detection was performed in the same way for all structures and states and was based on a previously described hippocampal ripple detection method[11,12]. Requirements for inclusion and criteria for rejection were determined using an iterative process across patients, structures, and states. Data were bandpassed at 60-120Hz and the top 20% of 20ms moving root-mean-squared peaks were detected. It was further required that the maximum z-score of the analytic amplitude of the 70-100Hz bandpass was greater than 3 and that there were at least 3 distinct oscillation cycles in the 120Hz lowpassed signal, determined by shifting a 40ms window in increments of 5ms across ±50ms relative to the ripple midpoint and requiring that at least 1 window have at least 3 peaks. Adjacent ripples within 25ms were merged. Ripple centers were determined as the time of the maximum positive peak in the 70-100Hz bandpass. To reject epileptiform activities or artifacts, ripples were excluded if the absolute value of the z-score of the 100Hz highpass exceeded 7 or if they occurred within 2s of a ≥1mV/ms change in the LFP. Ripples were also excluded if they fell within ±500ms of putative interictal spikes, detected as described below. To exclude events that could be coupled across channels due to epileptiform activity, we excluded ripples that coincided with a putative interictal spike on any cortical or hippocampal SEEG or ECoG channel included in the analyses. Events in SEEG and ECoG recordings that had only one prominent cycle or deflection in the broadband LFP that manifested as multiple cycles above detection threshold in the 70-100Hz bandpass were excluded if the largest valley-to-peak or peak-to-valley absolute amplitude in the broadband LFP was 2.5 times greater than the third largest. For each channel, the mean ripple-locked LFP and mean ripple band were visually examined to confirm that there were multiple prominent cycles at ripple frequency (70-100Hz) and the mean time-frequency plot was examined to confirm there was a distinct increase in power within the 70-100Hz band. In addition, multiple individual ripples in the broadband LFP and 70-100Hz bandpass from each channel were visually examined to confirm that there were multiple cycles at ripple frequency without contamination by artifacts or epileptiform activity. Channels that did not contain ripples that meet these criteria were excluded from the study.

Interictal spike detection and rejection

Ripples and sleep graphoelements were excluded if they were within ±500ms from putative IIS detected as follows. A high frequency score was computed by smoothing the 70-190Hz analytic amplitude with a 20ms boxcar function and a spike template score was generated by computing the cross-covariance with a template interictal spike. The high frequency score was weighted by 13 and the spike score was weighted by 25, and an IIS was detected when these weighted sums exceeded 130. In each patient, detected IIS and intervening epochs were visually examined from hippocampal (when included) and cortical channels to confirm high detection sensitivity and specificity.

Sleep graphoelement detection

Downstates and upstates were detected as previously described[11,12], where data from each channel were bandpassed from 0.1-4Hz (zero-phase shift) and consecutive zero crossings separated by 0.25-3s were selected. The top 10% amplitude peaks were selected and the polarity of each signal was inverted if needed so that downstates were negative and upstates were positive by confirming that the average analytic amplitude of the 70-190Hz bandpass ±100ms around peaks was greater for upstates than downstates.

Spindles were detected as previously described[53], where data were bandpassed at 10-16Hz, then the absolute values were smoothed via convolution with a tapered 300ms Tukey window, and median values were subtracted from each channel. Data were normalized by the median absolute deviation and spindles were detected when peaks exceeded 1 for at least 400ms. Onsets and offsets were marked when these amplitudes fell below 1. Putative spindles that coincided with large increases in lower (4-8Hz) or higher (18-25Hz) band power were rejected to exclude broadband events as well as theta bursts, which may extend into the lower end of the spindle range[21].

Ripple temporal relationships

Peri-cortical ripple time histograms of cortical graphoelements or Motif high gamma peaks on the same channel were computed. Gaussian smoothed (250ms window) event counts were found in 50ms bins for graphoelements within ±1500ms around cortical ripple centers at t=0. A null distribution was generated by shuffling the event times relative to the ripples at t=0 within this 3s window 200 times per channel. Pre-FDR p-values were computed by comparing the observed and null distributions within each bin over ±1000ms. These p-values were then FDR-corrected across bins and channels[54]. A channel was considered to have a significant modulation if it had 3 or more consecutive bins with FDR-corrected p-values less than α=0.05. Whether events were leading or lagging cortical ripples at t=0 was computed for each channel with a two-sided binomial test with expected value of 0.5, using event counts in the 1000ms before vs. 1000ms after t=0. Plots had 50ms Gaussian smoothed event counts with 50ms bins.

Conditional probabilities of a ripple given the following graphoelements or their sequences were computed: downstate, spindle, upstate, downstate–spindle, and spindle–upstate. A ripple given a spindle (R | SS) was determined if the ripple center occurred during the spindle (average spindle duration was 634ms). A ripple was considered to precede an upstate or follow a downstate if the ripple center occurred 634ms before or after the peak of the upstate or downstate, respectively.

Unit detection, classification, quality, and isolation

Unit detection and classification was performed according to our published procedures[24,55-60]. Data were bandpassed at 300-3000Hz and putative unit spikes were detected when the filtered signal exceeded 5 times the estimated standard deviation of the background noise. Units were k-means clustered using the first three principal components of each spike. Overlaid spikes were examined visually and those with abnormal waveforms were excluded. Based on their waveforms, firing rates, and autocorrelograms, action potentials were clustered as arising from putative pyramidal cells or interneurons. Putative pyramidal cells had spike rates of ~0.1-0.8Hz, long valley-to-peak and half width intervals, sharp autocorrelations, and bimodal inter-spike interval (ISI) distributions, reflecting a propensity to fire in bursts (STable 4). By contrast,

putative interneurons had spike rates of ~1-5Hz, short valley-to-peak and half width intervals, broad autocorrelations, and a predominantly unimodal ISI distribution.

Single unit quality and isolation were confirmed according to previously established guidelines[61]. Unit spikes were verified to well-exceed the noise floor based on large peak signal-to-noise ratios (SFig.4A). Since the neuronal spiking refractory period is about 3ms, the percent of ISIs less than 3ms estimates the degree of single unit contamination by spikes from different units, which was very low among the units included in this study (SFig.4B). Furthermore, single units detected on the same contact were highly separable according to their projection distances[62] (SFig.4C). Lastly, temporal stability of unit spikes over time was confirmed based on consistency of the mean waveform shape and amplitude of each unit across recording quartiles.

Analyses of unit spiking during ripples

Unit spiking was analyzed with respect to local ripples detected on the same contact. Ripple phases of unit spikes were determined by finding the angle of the Hilbert transform of the 70-100Hz bandpassed signal (zero phase shift) at the times of the spikes. The circular mean ripple phase was determined for each unit[63]. Phase analyses were only performed on units that had at least 30 spikes during local ripples. PY-PY and PY-IN unit pair co-firing within 5ms was assessed based on our previously published method[24]. To evaluate co-firing when there was a ripple at either or both sites vs. baseline when there were no ripples occurring, we randomly selected non-ripple epochs matched in number and duration to the ripples but during which there were no ripples detected on either channel. Co-firing during ripples with observed vs. random spike times was computed by shuffling the spike times of each unit within the ripple epochs.

Cortical replay analyses

We performed new analyses on data from subjects 2-4 in Jiang et al., (2017)[29] (STable 5). Analyses were performed on “Events” that were sequences of high gamma (70-190Hz) peaks identified during waking that recurred during the following NREM sleep, and which were considered ‘exact matches,’ such that all common channels had the same temporal order. Events consisting of high gamma peaks were identified as follows: outlier high gamma peaks were counted in 2s windows moving in 50ms increments. Events were identified when windows had local maxima of high gamma outlier peaks (minimum 4). When there were multiple high gamma peaks from the same channel during a given Event, only the median high gamma peak position across these channels was used.
Spatiotemporal Motifs were selected using methods from rat cortical electrophysiology studies. Events were grouped according to spatial distribution similarity in R with the packages Fast Hierarchical Clustering Routine[64] and Dynamic Tree Cut[65] using Phi-coefficient-derived distance matrices[66] and Ward’s method[64]. Motifs, which occurred during waking and NREM sleep, were identified by grouping waking Events based on high gamma peak order and then matching them to NREM Events. Temporal order similarity for waking Events in each cluster was computed using the matching index (MI) algorithm, which was implemented as previously described[5], except using high gamma peaks in place of spike train convolutions in MATLAB with custom scripts and in R with the TraMineR toolbox[67], with an additional heuristic criterion that only the channels in common for each comparison were used to calculate MI. This metric of pattern similarity required that each channel had a unique position in the sequence since channel pair orders were compared with the MI.

Each cluster of spatially similar waking Events was subsequently divided into subclusters. Motifs that included 90% of a given subcluster's Events in their neighborhoods, defined as 20% of the maximum distance between two Events for a given subcluster, were selected. These were then matched with MI to the Events in NREM sleep, and each representative was associated with a certain number of replay frames (i.e., NREM Events that matched the waking Motif, or "Motif-Event matches") for each NREM period. If multiple Motifs matched to the same NREM Event the number of replay frames associated with each waking Motif for that night was incremented by $1/N$ instead of 1, where N was the number of waking Motifs matched to the Event. Therefore, the total increments from any given Event was equal to 1 regardless of the number of matching Motifs as long as there was at least one match. The resulting replay frame numbers for each NREM period were then normalized by the total number of Events found in that NREM period. Waking motifs were required to match at least 2 Events.

Counts were made for Motifs that had more Motif-Event matches during the preceding than following NREM sleeps. This was compared to the number with the reverse pattern with a two-sided binomial test with an expected value of 0.5. Motifs were only included if their total number of NREM Event matches across all 4 nights (2 preceding waking, 2 following) exceeded Motif-wise thresholds established by matching preceding sleep and post sleep Event to the same Motifs with the channel order randomly shuffled 1000 times.

Statistical analyses

All statistical tests were evaluated with $\alpha=0.05$. *P*-values involving multiple comparisons were FDR-corrected[54] as specified in the text. Box-and-whisker plots show median, mean, and interquartile range, with whiskers indicating 1.5 × interquartile range, and with outliers omitted. Significance of linear correlations were assessed using the significance of the correlation coefficient when there were at least 10 data points.

Data availability

The de-identified raw data that support the findings of this study are available from the corresponding authors upon reasonable request provided that the data sharing agreement and patient consent permit that sharing.

Code availability

The code that support the findings of this study are available from the corresponding authors upon reasonable request.

References

1 Wilson, M. A. & McNaughton, B. L. Reactivation of hippocampal ensemble memories during sleep. *Science* **265**, 676-679 (1994).

2 Buzsaki, G. Hippocampal sharp wave-ripple: A cognitive biomarker for episodic memory and planning. *Hippocampus* **25**, 1073-1188, doi:doi:10.1002/hipo.22488 (2015).

3 Maingret, N., Girardeau, G., Todorova, R., Goutierre, M. & Zugaro, M. Hippocampo-cortical coupling mediates memory consolidation during sleep. *Nature Neuroscience* **19**, 959-964, doi:10.1038/nn.4304 (2016).

4 Ego-Stengel, V. & Wilson, M. A. Disruption of ripple-associated hippocampal activity during rest impairs spatial learning in the rat. *Hippocampus* **20**, 1-10, doi:10.1002/hipo.20707 (2009).

5 Ji, D. & Wilson, M. A. Coordinated memory replay in the visual cortex and hippocampus during sleep. *Nature Neuroscience* **10**, 100-107, doi:10.1038/nn1825 (2007).

6 Peyrache, A., Khamassi, M., Benchenane, K., Wiener, S. I. & Battaglia, F. P. Replay of rule-learning related neural patterns in the prefrontal cortex during sleep. *Nature Neuroscience* **12**, 919-926, doi:10.1038/nn.2337 (2009).

7 Johnson, L. A., Euston, D. R., Tatsuno, M. & McNaughton, B. L. Stored-trace reactivation in rat prefrontal cortex is correlated with down-to-up state fluctuation density. *J Neurosci* **30**, 2650-2661, doi:10.1523/JNEUROSCI.1617-09.2010 (2010).

8 Siapas, A. G. & Wilson, M. A. Coordinated interactions between hippocampal ripples and cortical spindles during slow-wave sleep. *Neuron* **21**, 1123-1128 (1998).

9 Latchoumane, C.-F. V., Ngo, H.-V. V., Born, J. & Shin, H.-S. Thalamic Spindles Promote Memory Formation during Sleep through Triple Phase-Locking of Cortical, Thalamic, and Hippocampal Rhythms. *Neuron* **95**, 424-435.e426, doi:10.1016/j.neuron.2017.06.025 (2017).

10 Staresina, B. P. *et al.* Hierarchical nesting of slow oscillations, spindles and ripples in the human hippocampus during sleep. *Nature Neuroscience* **18**, 1679-1686, doi:10.1038/nn.4119 (2015).

11 Jiang, X., Gonzalez-Martinez, J. & Halgren, E. Coordination of Human Hippocampal Sharpwave Ripples during NREM Sleep with Cortical Theta Bursts, Spindles, Downstates, and Upstates. *J Neurosci* **39**, 8744-8761, doi:10.1523/jneurosci.2857-18.2019 (2019).

12 Jiang, X., Gonzalez-Martinez, J. & Halgren, E. Posterior hippocampal spindle-ripples co-occur with neocortical theta-bursts and down-upstates, and phase-lock with parietal spindles during NREM sleep in humans. *J Neurosci*, 2858-2818, doi:10.1523/jneurosci.2858-18.2019 (2019).

13 Jiang, X. *et al.* Improved identification and differentiation from epileptiform activity of human hippocampal sharp wave ripples during NREM sleep. *Hippocampus* (2019).

14 Khodagholy, D., Gelinas, J. N. & Buzsáki, G. Learning-enhanced coupling between ripple oscillations in association cortices and hippocampus. *Science* **358**, 369-372, doi:10.1126/science.aan6203 (2017).

15 Grenier, F., Timofeev, I. & Steriade, M. Focal synchronization of ripples (80-200 Hz) in neocortex and their neuronal correlates. *J Neurophysiol* **86**, 1884-1898. (2001).

16 Vaz, A. P., Inati, S. K., Brunel, N. & Zaghloul, K. A. Coupled ripple oscillations between the medial temporal lobe and neocortex retrieve human memory. *Science* **363**, 975-978 (2019).

17 Vaz, A. P., Wittig, J. H., Inati, S. K. & Zaghloul, K. A. Replay of cortical spiking sequences during human memory retrieval. *Science* **367**, 1131-1134 (2020).

18 Norman, Y. *et al.* Hippocampal sharp-wave ripples linked to visual episodic recollection in humans. *Science* **365**, eaax1030 (2019).

19 Mukamel, R. *et al.* Coupling between neuronal firing, field potentials, and FMRI in human auditory cortex. *Science* **309**, 951-954, doi:10.1126/science.1110913 (2005).
20 Rosen, B. Q. & Halgren, E. A whole-cortex probabilistic diffusion tractography connectome. *eNeuro*, ENEURO.0416-0420.2020, doi:10.1523/eneuro.0416-20.2020 (2021).
21 Gonzalez, C. E. *et al.* Theta bursts precede, and spindles follow, cortical and thalamic downstates in human NREM sleep. *J Neurosci* **38**, 9989-10001 (2018).
22 Mak-McCully, R. A. *et al.* Coordination of cortical and thalamic activity during non-REM human sleep. *Nature Communications* (2017).
23 Csercsa, R. *et al.* Laminar analysis of slow wave activity in humans. *Brain* **133**, 2814-2829, doi:10.1093/brain/awq169 (2010).
24 Dickey, C. W. *et al.* Travelling spindles create necessary conditions for spike-timing-dependent plasticity in humans. *Nature Communications* **12**, 1027, doi:10.1038/s41467-021-21298-x (2021).
25 Bazhenov, M., Rulkov, N. F. & Timofeev, I. Effect of synaptic connectivity on long-range synchronization of fast cortical oscillations. *J Neurophysiol* (2008).
26 Stark, E. *et al.* Pyramidal cell-interneuron interactions underlie hippocampal ripple oscillations. *Neuron* **83**, 467-480, doi:10.1016/j.neuron.2014.06.023 (2014).
27 Buzsáki, G. & Wang, X. J. Mechanisms of gamma oscillations. *Annu Rev Neurosci* **35**, 203-225, doi:10.1146/annurev-neuro-062111-150444 (2012).
28 Rasch, B. & Born, J. About sleep's role in memory. *Physiol Rev* **93**, 681-766, doi:10.1152/physrev.00032.2012 (2013).
29 Jiang, X. *et al.* Replay of large-scale spatio-temporal patterns from waking during subsequent NREM sleep in human cortex. *Scientific Reports* **7**, 17380, doi:10.1038/s41598-017-17469-w (2017).
30 Bartos, M. *et al.* Fast synaptic inhibition promotes synchronized gamma oscillations in hippocampal interneuron networks. *Proceedings of the National Academy of Science* **99**, 13222-13227. (2002).
31 Feldman, D. E. The spike-timing dependence of plasticity. *Neuron* **75**, 556-571 (2012).
32 Fernández, E. *et al.* Acute human brain responses to intracortical microelectrode arrays: challenges and future prospects. *Frontiers in Neuroengineering* **7**, doi:10.3389/fneng.2014.00024 (2014).
33 Keller, C. J. *et al.* Heterogeneous neuronal firing patterns during interictal epileptiform discharges in the human cortex. *Brain* **133**, 1668-1681, doi:10.1093/brain/awq112 (2010).
34 Waziri, A. *et al.* Initial surgical experience with a dense cortical microarray in epileptic patients undergoing craniotomy for subdural electrode implantation. *Neurosurgery* **64**, 540-545; discussion 545, doi:10.1227/01.NEU.0000337575.63861.10 (2009).
35 Oostenveld, R., Fries, P., Maris, E. & Schoffelen, J. M. FieldTrip: Open source software for advanced analysis of MEG, EEG, and invasive electrophysiological data. *Comput Intell Neurosci* **2011**, 156869, doi:10.1155/2011/156869 (2011).
36 Mak-McCully, R. A. *et al.* Distribution, Amplitude, Incidence, Co-Occurrence, and Propagation of Human K-Complexes in Focal Transcortical Recordings. *eNeuro* **2**, doi:10.1523/eneuro.0028-15.2015 (2015).
37 Fischl, B. FreeSurfer. *Neuroimage* **62**, 774-781, doi:10.1016/j.neuroimage.2012.01.021 (2012).
38 Fischl, B. *et al.* Automatically parcellating the human cerebral cortex. *Cereb Cortex* **14**, 11-22, doi:10.1093/cercor/bhg087 (2004).
39 Destrieux, C., Fischl, B., Dale, A. & Halgren, E. Automatic parcellation of human cortical gyri and sulci using standard anatomical nomenclature. *Neuroimage* **53**, 1-15, doi:10.1016/j.neuroimage.2010.06.010 (2010).

40 Iglesias, J. E. *et al.* A computational atlas of the hippocampal formation using ex vivo, ultra-high resolution MRI: Application to adaptive segmentation of in vivo MRI. *Neuroimage* **115**, 117-137, doi:10.1016/j.neuroimage.2015.04.042 (2015).
41 Johnson, H., Harris, G. & Williams, K. BRAINSFIT: Mutual information registrations of whole-brain 3D Images, using the insight toolkit. (2007).
42 Fedorov, A. *et al.* 3D Slicer as an image computing platform for the Quantitative Imaging Network. *Magn Reson Imaging* **30**, 1323-1341, doi:10.1016/j.mri.2012.05.001 (2012).
43 Fischl, B., Sereno, M. I., Tootell, R. B. & Dale, A. M. High-resolution intersubject averaging and a coordinate system for the cortical surface. *Hum Brain Mapp* **8**, 272-284, doi:10.1002/(sici)1097-0193(1999)8:4<272::aid-hbm10>3.0.co;2-4 (1999).
44 Desikan, R. S. *et al.* An automated labeling system for subdividing the human cerebral cortex on MRI scans into gyral based regions of interest. *NeuroImage* **31**, 968-980 (2006).
45 Glasser, M. F. & Van Essen, D. C. Mapping human cortical areas in vivo based on myelin content as revealed by T1- and T2-weighted MRI. *J Neurosci* **31**, 11597-11616, doi:10.1523/JNEUROSCI.2180-11.2011 (2011).
46 Glasser, M. F. *et al.* A multi-modal parcellation of human cerebral cortex. *Nature* (2016).
47 Delorme, A. & Makeig, S. EEGLAB: an open source toolbox for analysis of single-trial EEG dynamics including independent component analysis. *J Neurosci Methods* **134**, 9-21, doi:10.1016/j.jneumeth.2003.10.009 (2004).
48 Axmacher, N., Elger, C. E. & Fell, J. Ripples in the medial temporal lobe are relevant for human memory consolidation. *Brain* **131**, 1806-1817 (2008).
49 Le Van Quyen, M. *et al.* Cell Type-Specific Firing during Ripple Oscillations in the Hippocampal Formation of Humans. *J Neurosci* **28**, 6104-6110, doi:10.1523/jneurosci.0437-08.2008 (2008).
50 Clemens, Z. *et al.* Temporal coupling of parahippocampal ripples, sleep spindles and slow oscillations in humans. *Brain* **130**, 2868-2878, doi:10.1093/brain/awm146 (2007).
51 Staba, R. J. *et al.* High-frequency oscillations recorded in human medial temporal lobe during sleep. *Annals of Neurology* **56**, 108-115, doi:doi:10.1002/ana.20164 (2004).
52 Bragin, A., Engel, J., Jr., Wilson, C. L., Fried, I. & Buzsaki, G. High-frequency oscillations in human brain. *Hippocampus* **9**, 137-142 (1999).
53 Hagler, D. J., Jr. *et al.* Heterogeneous Origins of Human Sleep Spindles in Different Cortical Layers. *J Neurosci* **38**, 3013-3025, doi:10.1523/jneurosci.2241-17.2018 (2018).
54 Benjamini, Y. & Hochberg, Y. Controlling the false discovery rate: a practical and powerful approach to multiple testing. *Journal of the Royal statistical society: series B (Methodological)* **57**, 289-300 (1995).
55 Eichenlaub, J.-B. *et al.* Replay of Learned Neural Firing Sequences during Rest in Human Motor Cortex. *Cell Reports* **31**, 107581 (2020).
56 Teleńczuk, B. *et al.* Local field potentials primarily reflect inhibitory neuron activity in human and monkey cortex. *Scientific reports* **7**, 40211 (2017).
57 Le Van Quyen, M. *et al.* High-frequency oscillations in human and monkey neocortex during the wake–sleep cycle. *Proceedings of the National Academy of Sciences* **113**, 9363-9368 (2016).
58 Dehghani, N. *et al.* Dynamic balance of excitation and inhibition in human and monkey neocortex. *Scientific Reports* **6** (2016).
59 Chan, A. M. *et al.* Speech-specific tuning of neurons in human superior temporal gyrus. *Cereb Cortex* **24**, 2679-2693, doi:10.1093/cercor/bht127 (2014).
60 Peyrache, A. *et al.* Spatiotemporal dynamics of neocortical excitation and inhibition during human sleep. *Proceedings of the National Academy of Science* **109**, 1731-1736, doi:10.1073/pnas.1109895109 (2012).

61 Kamiński, J., Brzezicka, A., Mamelak, A. N. & Rutishauser, U. Combined Phase-Rate Coding by Persistently Active Neurons as a Mechanism for Maintaining Multiple Items in Working Memory in Humans. *Neuron* **106**, 256-264.e253, doi:10.1016/j.neuron.2020.01.032 (2020).
62 Pouzat, C., Mazor, O. & Laurent, G. Using noise signature to optimize spike-sorting and to assess neuronal classification quality. *Journal of Neuroscience Methods* **122**, 43-57, doi:10.1016/S0165-0270(02)00276-5 (2002).
63 Berens, P. CircStat: A MATLAB Toolbox for Circular Statistics. *Journal of Statistical Software* **31**, 1-21, doi:10.18637/jss.v031.i10 (2009).
64 Müllner, D. fastcluster: Fast hierarchical, agglomerative clustering routines for R and Python. *Journal of Statistical Software* **53**, 1-18 (2013).
65 Langfelder, P., Zhang, B. & Horvath, S. Defining clusters from a hierarchical cluster tree: the Dynamic Tree Cut package for R. *Bioinformatics* **24**, 719-720, doi:10.1093/bioinformatics/btm563 (2008).
66 Miller, J.-e. K., Ayzenshtat, I., Carrillo-Reid, L. & Yuste, R. Visual stimuli recruit intrinsically generated cortical ensembles. *Proceedings of the National Academy of Sciences* **111**, E4053-E4061 (2014).
67 Gabadinho, A., Ritschard, G., Mueller, N. S. & Studer, M. Analyzing and visualizing state sequences in R with TraMineR. *Journal of Statistical Software* **40**, 1-37 (2011).